Cell-Type-Specific Cytokinin Distribution within the Arabidopsis Primary Root Apex[OPEN]

Ioanna Antoniadi,[a,b,1] Lenka Plačková,[c,1] Biljana Simonovik,[a] Karel Doležal,[c] Colin Turnbull,[b] Karin Ljung,[a,2] and Ondřej Novák[c,2,3]

[a] Umeå Plant Science Centre, Department of Forest Genetics and Plant Physiology, Swedish University of Agricultural Sciences, SE-901 83 Umeå, Sweden
[b] Department of Life Sciences, Imperial College London, London SW7 2AZ, United Kingdom
[c] Laboratory of Growth Regulators and Department of Chemical Biology and Genetics, Centre of the Region Haná for Biotechnological and Agricultural Research, Institute of Experimental Botany AS CR and Faculty of Science of Palacký University, Šlechtitelů 27, CZ-78371 Olomouc, Czech Republic

ORCID IDs: 0000-0001-9053-2788 (I.A.); 0000-0003-2537-4933 (L.P.); 0000-0002-0929-0791 (B.S.); 0000-0001-6635-1418 (C.T.); 0000-0003-2901-189X (K.L.); 0000-0003-3452-0154 (O.N.)

Cytokinins (CKs) play a crucial role in many physiological and developmental processes at the levels of individual plant components (cells, tissues, and organs) and by coordinating activities across these parts. High-resolution measurements of intracellular CKs in different plant tissues can therefore provide insights into their metabolism and mode of action. Here, we applied fluorescence-activated cell sorting of green fluorescent protein (GFP)-marked cell types, combined with solid-phase microextraction and an ultra-high-sensitivity mass spectrometry (MS) method for analysis of CK biosynthesis and homeostasis at cellular resolution. This method was validated by series of control experiments, establishing that protoplast isolation and cell sorting procedures did not greatly alter endogenous CK levels. The MS-based method facilitated the quantification of all the well known CK isoprenoid metabolites in four different transgenic *Arabidopsis thaliana* lines expressing GFP in specific cell populations within the primary root apex. Our results revealed the presence of a CK gradient within the Arabidopsis root tip, with a concentration maximum in the lateral root cap, columella, columella initials, and quiescent center cells. This distribution, when compared with previously published auxin gradients, implies that the well known antagonistic interactions between the two hormone groups are cell type specific.

INTRODUCTION

Plant hormones are signal molecules that are synthesized in many different tissues and cell types, and their actions span from cell-autonomous to short range to long distance. Understanding hormone function therefore requires detailed knowledge of the spatial regulation of biosynthesis, metabolism, transport, perception, and signal transduction. In this study, we focused on cytokinins, a class of hormone with multiple functions throughout the plant that interact with several other hormone classes including auxin, ethylene, abscisic acid, gibberellins, and strigolactones (El-Showk et al., 2013).

Cytokinins (CKs) are N^6-substituted adenines carrying an aliphatic side chain of isoprenoid origin (isoprenoid CKs) or an aromatic derivative side chain (aromatic CKs). Variation in structural substituents on the adenine moiety of CKs includes nucleotide forms, ribosides, and free bases, along with a wide range of other conjugates. It is widely believed that CK free bases are the

bioactive CKs (Schmitz and Skoog, 1972; Spiess, 1975; Sakakibara, 2006). However, in CK receptor binding assays, either in vitro or in in vivo heterologous expression systems, some ribosides also display high affinity with CK receptors (Spíchal et al., 2004; Yonekura-Sakakibara et al., 2004; Romanov et al., 2006). Moreover, bioassays showed activity of compounds such as CK-*O*-glucosides that are unable to bind to receptors (Spíchal et al., 2004; Gajdosová et al., 2011). Therefore, measurements of CK free bases alone do not provide a complete picture of bioactive and potentially bioactive CKs within tissues. In parallel, variations in the CK side chain and stereoisomeric configuration divide isoprenoid CKs into isopentenyladenine (iP), *trans*-zeatin (*t*Z), dihydrozeatin, and *cis*-zeatin (*c*Z) groups. While iP and *t*Z groups are considered the most important compounds (Sakakibara, 2006), the functional relevance of *c*Z-type CKs has been elevated within the last decade (Gajdosová et al., 2011; Köllmer et al., 2014).

Based on reporter gene expression studies, mainly performed in *Arabidopsis thaliana*, the genes encoding ISOPENTENYL TRANSFERASES (IPTs), catalyzing the first committed step of CK biosynthesis, are expressed in almost every part of the plant, but each *IPT* gene has a spatially distinct pattern of expression. For example, *IPT3* is expressed almost exclusively in the phloem, whereas *IPT5* expression is confined to root cap, columella, lateral root initials, floral stems, and silique abscission zones (Miyawaki et al., 2004; Takei et al., 2004). Similarly, genes encoding enzymes for CK activation (*LONELY GUY* [*LOG*] and cytochrome P450 family [*CYP735A*]) and degradation by cytokinin dehydrogenase

---

[1] These authors contributed equally to this work.
[2] These authors contributed equally to this work.
[3] Address correspondence to novako@ueb.cas.cz.

[OPEN]Articles can be viewed online without a subscription.

(*CYTOKININ OXIDASE/DEHYDROGENASE* [*CKX*]) also appear to be spatially regulated. In root tips, expression of *LOG3* and *LOG8* is strongest in the procambium and quiescent center (QC), respectively (Kuroha et al., 2009), whereas root expression of *CYP735A2* is predominantly in the vasculature (Kiba et al., 2013). Analysis of GUS patterns reveals that *CKX4* is expressed in guard cells and root cap, *CKX5* in axillary buds, and *CKX6* in phloem (Werner et al., 2003).

The evolutionary pressures that led to selection of such diversity and apparently exquisite precision of spatial patterns of expression are not yet clear. Despite the tight spatial regulation, there is substantial redundancy among gene family members, with minimal deleterious phenotypes seen in single and double *ipt* mutants and altered development only becoming highly apparent in triple and quadruple knockout lines (Miyawaki et al., 2006), suggesting that CKs produced elsewhere in the plant can cause complementation by compensation for local deficiencies. This can extend to systemic transport, as evidenced by complete rescue of *ipt1,3,5,7* quadruple mutant shoots by grafting to wild-type roots (Matsumoto-Kitano et al., 2008).

Relatively little is known about regulation of CK transport. Although PURINE UPTAKE PERMEASEs (PUPs) and EQUILIBRATIVE NUCLEOSIDE TRANSPORTERs (ENTs) can enable movement of CKs across membranes (Bürkle et al., 2003; Hirose et al., 2005), their biological importance remains to be fully ascertained. Genetic studies of both PUPs and ENTs are hampered by the large number of genes in each family and by the fact that the proteins appear also to transport non-CK purine molecules in addition to CKs. The ATP binding cassette transporter subfamily G14 (*ABCG14*) has recently been shown to regulate entry of zeatin-type CKs into the xylem transport stream and hence may function primarily in long-distance export from root to shoot rather than local transport (Ko et al., 2014; Zhang et al., 2014).

In relation to their spatially regulated effects on other hormones, there is convincing evidence that CKs, at least when supplied exogenously, modulate auxin *PIN* transporter expression and distribution (Růžička et al., 2009; Zhang et al., 2011; Marhavý et al., 2014), and CKs also affect auxin biosynthesis rates in several root cell types (Jones et al., 2010).

As many forms of CKs are potentially mobile intercellular signals, knowledge of sites of biosynthesis does not necessarily reflect sites of maximal accumulation and biological action. To reveal the pattern of CK distribution among different cell types, we used a combination of fluorescence-activated cell sorting (FACS) and ultra-high-performance liquid chromatography-tandem mass spectrometry (UHPLC-MS/MS) to analyze the CK metabolite content of a range of green fluorescent protein (GFP)-marked cell types isolated from the Arabidopsis root apex, an approach previously used to generate a high-resolution map of auxin (indole-3-acetic acid [IAA]) biosynthesis and distribution (Petersson et al., 2009). Validation and control experiments revealed that the CK amounts of protoplasts generally changed very little over the time required to generate and collect different cell populations, and only small proportions of CKs were lost by leakage from the protoplasts. Because CKs exist in multiple molecular forms and their levels are generally much lower than that of IAA, an ultra-high-sensitive UHPLC-MS/MS method was developed to detect 26 known isoprenoid CKs. This revealed that CK distribution was similar across some of the tested cell types (stele, endodermis, epidermis, and cortex) but significantly enhanced in the cell population that contained the lateral root cap, columella, columella initials, and the quiescent center. This study, along with similar studies of IAA and its catabolite 2-oxindole-3-acetic acid (Petersson et al., 2009; Pěnčík et al., 2013), complements transcriptional analyses performed at the cell-specific level in the Arabidopsis root tip (Birnbaum et al., 2003, 2005; Brady et al., 2007) and brings us closer to mapping the details of gene-hormone regulation in complex plant organs comprising multiple cell types in close proximity.

RESULTS

To quantify CKs in specific cell populations of the Arabidopsis root apex, an efficient protoplast isolation and cell sorting process was required. Moreover, in order to profile all different types of CK metabolites in these cell populations, a sensitive and selective method for CK analysis was developed, based on solid-phase microextraction (microSPE) and mass spectrometry-based quantification. To test whether these procedures alter endogenous CK levels, a series of control experiments was conducted.

The Protoplast Isolation Process Does Not Greatly Alter Endogenous Cytokinin Levels

To obtain free protoplasts for cell sorting and subsequent CK analysis, the cell walls were removed by incubating Arabidopsis roots in a medium containing cell wall-degrading enzymes. To examine the possible effects of protoplast isolation on CK metabolism, chemical treatments were applied during the 2 h of enzymatic degradation of the cell walls. Inhibiting CK irreversible degradation with 2-chloro-6-(3-methoxyphenyl)aminopurine (INCYDE) (Zatloukal et al., 2008; Aremu et al., 2012) resulted in elevated levels of the CK bases iP and *t*Z and the riboside iPR, while *c*Z levels were reduced (Figure 1A). Treatments with adenine, previously used as a cytokinin transport antagonist (Bürkle et al., 2003; Cedzich et al., 2008), mainly caused a small decrease of all CK bases detected and slightly increased levels of all ribosides (Figure 1B). When sodium azide was added to the protoplast isolation buffer as an inhibitor of ATP-dependent metabolic and membrane transport processes (Tucker, 1993), iPR level was elevated while tZR concentration was reduced (Figure 1C). Taken together, the data derived from these chemical treatments suggest that during protoplast isolation, measured CK levels still broadly represent the endogenous hormone concentrations. Moreover, these slight alterations in CK content indicate that active CK homeostasis continues to operate in the isolated cells.

Cytokinin Leakage and Transport Is Minimal during Cell Sorting

The effect of the cell sorting procedure on endogenous CK levels was also determined. The isolated protoplasts were suspended in 0.7% NaCl (sorting buffer) and kept at 4°C for 180 min, imitating the sorting process. The CK metabolites were quantified after 0, 90, and 180 min in the protoplast pellet and in the respective supernatant to check for possible leakage and/or transport of CKs into the medium.
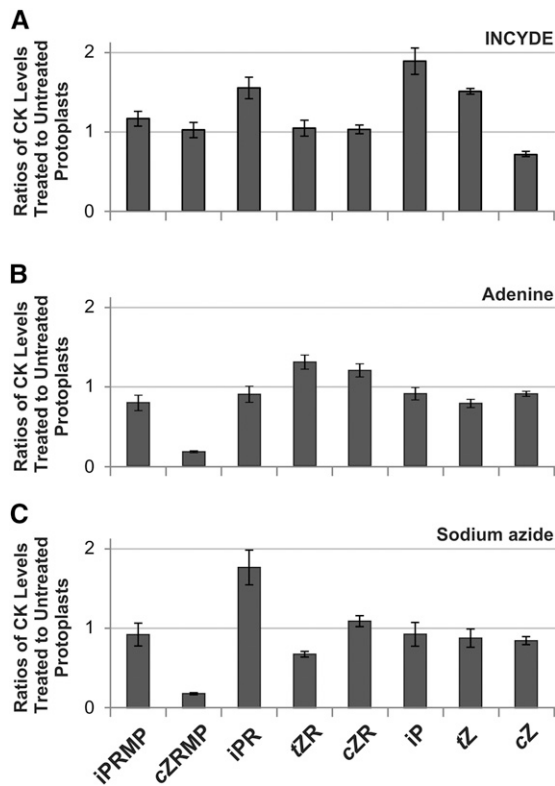
Figure 1. Cytokinin Concentration in Isolated Protoplasts.

Roots from seedlings 8 d after germination were treated with or without 10 μM INCYDE (a cytokinin dehydrogenase inhibitor; **[A]**), 100 μM adenine (a cytokinin transport antagonist; **[B]**), or 3 mM sodium azide (an inhibitor of ATP-dependent metabolic and membrane transport processes; **[C]**) during protoplast isolation (2 h). The CK concentration was calculated as fmol/100,000 protoplasts, and the respective ratios (treated to untreated) were then determined. Three biological replicates were analyzed for each treatment, and for each replicate at least 1500 roots of wild-type Arabidopsis plants (Col-0) were pooled. Error bars indicate SE.

The distribution of CK metabolites in the protoplasts, presented in Figure 2A, remained largely stable during the 3 h of incubation at 4°C, suggesting that there is no major net leakage and/or transport of CKs out of the protoplasts over this period. The CK levels detected in the corresponding supernatants of the protoplast samples, shown in Figure 2B, are likely to be derived from partially digested cell walls and damaged protoplasts. Again, negligible alterations in the CK profiles of the supernatants were observed over time. Taken together, these data indicate that there are only slight modifications of CK levels and metabolism during the sorting procedure (Figure 2C).

Miniaturized SPE Efficiently Purifies CK Metabolites from Isolated Protoplasts

Inspired by the high selectivity, affinity, and capacity of the multi-StageTip sorbents (Svačinová et al., 2012), we optimized the micropurification step as a powerful, one-step high-throughput approach for analysis of complex CK profiles from isolated protoplasts. We first compared the extraction capability

of multi-StageTip microcolumns packed with one, two, and three layers of each sorbent with the capacity of commercially available mixed-mode cation-exchange (MCX) phase (Dobrev and Kamínek, 2002). As shown in Supplemental Figure 1A, both purification protocols exhibited similar extraction efficiencies toward CKs, indicating that CKs could also be effectively enriched by in-tip microSPE from minute samples such as isolated cell populations. Altogether, total extraction recoveries (76% ± 15%, 82% ± 12%, and 81% ± 9% for one, two and three layers of each sorbent) were in good agreement with the excellent recovery, high reproducibility, and robustness of the commonly used MCX purification method (82% ± 6%). The increasing amount and surface area of sorbent multilayers positively affected the extraction yields of CK nucleotides (Supplemental Figure 1A); hence, three-layer StageTip microcolumns were chosen for purification of CKs from isolated protoplasts.
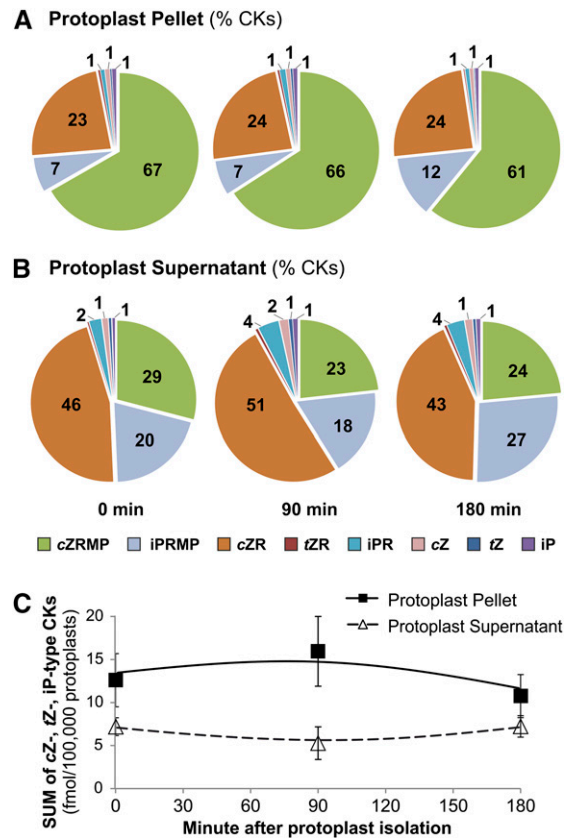

Figure 2. Cytokinin Metabolite Profiles in Protoplast Pellet and Supernatant.

Isolated protoplasts were suspended in sorting buffer and left on ice during simulated sorting for up to 180 min. Samples were collected every 90 min, centrifuged, and processed for separate analysis of the CK content in the protoplast pellet and supernatant. Nucleotides, ribosides, and bases of iP and cis- and trans-zeatin were quantified as fmol/100,000 protoplasts. Their percentage proportional distributions (**[A]** and **[B]**) and their sum **(C)** were calculated. For each time point, three biological replicates were assessed, and every replicate was derived from a pool of at least 1500 roots of wild-type Arabidopsis plants (Col-0). Error bars indicate SE.

As described above, the isolated protoplasts were suspended in 0.7% NaCl (sorting buffer), which is not compatible with LC-MS analysis. The large excess of sodium ions could result in the formation of metal adduct ion species, limiting ionization efficiency and thus reducing sensitivity of mass spectrometry detection. Moreover, the presence of NaCl in the sorting buffer might also have a detrimental effect on the process efficiency of the microSPE protocol, especially because high concentrations of chloride anions compete with CKs for the binding sites of the stationary phases used and thus decreasing mainly the recovery of CK nucleotides. Therefore, the initial extraction conditions (sorbent activation/ equilibration and sample loading) were optimized (Supplemental Figures 1B and 1C). Following a published microSPE protocol (Svačinová et al., 2012), the activation of C_{18}/SDB-RPS/Cation-SR layers by nondiluted/diluted solutions of 50% (v/v) nitric acid and 1 M formic acid was examined using 0.1 pmol of each CK metabolite spiked in before extraction. Conditioning with strong nitric acid enabled the sorbents to interact more efficiently with the sample matrix, giving close to 60% process efficiency (Supplemental Figure 1B). Simultaneously testing dilutions of 0.7% NaCl solution on the sample loading step showed that most of the tested CK metabolites were strongly retained using sorting buffer diluted with water (ratio 3:1) (Supplemental Figure 1C). Supplemental Figure 2 describes the final optimized in-tip microSPE protocol used for purification of CKs from isolated protoplasts.

A Methodology for High-Resolution Cell-Specific Analysis of Cytokinin Distribution

After optimizing the microSPE protocol and validation of protoplast isolation and sorting steps, we were able to quantify CK metabolites in the apical root cell types under study. These included the tissues of epidermis and cortex (J2812:GFP expression), stele (pWOODEN LEG:GFP [pWOL:GFP] expression), endodermis and QC (pSCARECROW:GFP [pSCR:GFP] expression) and lateral root cap, columella, columella initials, and QC cells (M0028:GFP expression) as also shown in Figure 3A. Root protoplasts were isolated from 8-d-old Arabidopsis seedlings expressing GFP in the specific cell types mentioned above and thus covering all the cell types of the root apex. The isolated protoplasts were then sorted using FACS into GFP-expressing (GFP⁺) and non-GFP-expressing (GFP⁻) protoplasts, with the latter representing a specific reference population for each sample (Figure 3B). For three of the transgenic lines analyzed, two samples of 200,000 GFP⁺ and GFP⁻ cells were collected during each sorting procedure (two technical replicates) and at least six cell-sorting experiments were performed for each Arabidopsis line (6 to 10 biological replicates). For the M0028:GFP line, a total of 20,000 to 100,000 isolated protoplasts were collected for each biological and technical replicate (for both the GFP⁺ and GFP⁻ cell populations). Commercial sorting buffers with unknown composition were replaced by 0.7% NaCl solution to minimize sample matrix effects. Known composition of the sorting buffer was also useful during further optimization of the subsequent microSPE step, as mentioned above (Figure 3C). After sample purification, the levels of known isoprenoid CKs were measured in both the GFP⁺ and GFP⁻ samples using ultra-high-sensitive and selective UHPLC-MS/MS (Supplemental Table 1). Finally, the CK concentration in the GFP⁺ cells of each line was normalized according to the respective GFP⁻ reference population.

Cytokinin Concentrations in Arabidopsis Root Cell Types

Fifteen different cytokinins, representing three basic isoprenoid side chain types (tZ, cZ, and iP) were successfully quantified in the sorted cells (Supplemental Figure 3). In the GFP⁺ and GFP⁻ protoplast populations, the CK nucleotides (iPRMP and cZRMP), the CK ribosides (iPR and cZR), the CK bases (iP, tZ, and cZ), and the CK 7-/9-/O-glucoside conjugates (iP7G, iP9G, tZ7G, tZ9G, cZ9G, tZOG, and cZOG) were detected, whereas cZROG was found only in the GFP nonexpressing cells of the pSCR:GFP and M0028:GFP lines. All the CK bases, ribosides, and 7-glucosides detected were present in all cell types under study. On the other hand, some cell lines lacked some nucleotides and O- and 9-glucoside forms. Interestingly, tZRMP and tZR were neither detected in the GFP⁺ nor the GFP⁻ cells (Supplemental Figure 3).

The levels of CK metabolites ranged from 0.3 to 10 fmol per 100,000 sorted cells depending on the cell types sorted from the root apex. Expressed as total CK concentrations, 5.5 ± 2.2, 2.4 ± 0.9, 17.9 ± 3.0, and 29.0 ± 8.1 fmol/100,000 protoplasts were found in GFP⁺ cells isolated from J2812:GFP, pWOL:GFP, pSCR: GFP, and M0028:GFP lines, respectively (Supplemental Figure 4A). The iP and cZ forms were the most abundant CK groups, with tZ forms present at approximately 5-fold lower concentrations (Supplemental Figure 4C). Surprisingly, only slight changes in overall CK metabolite distribution (from 1 to 6%) were observed between the GFP⁺ and GFP⁻ protoplast populations (Supplemental Figure 3). As mentioned above, a wide spectrum of CK metabolite groups was detected in GFP-expressing cells. Moreover, the highest concentrations of CK nucleotides, ribosides, and CK N-/O-glucosyl conjugates (around 50%) were found in the M0028:GFP cell population representing lateral root cap, columella, columella initials, and QC cells. In contrast, the concentration of CK bases (sum of iP, tZ, and cZ) was the highest in the endodermis (pSCR:GFP population) followed closely by CK nucleotides (Supplemental Figure 4B).

Altogether, the CK concentration map presented in Supplemental Figure 4 demonstrates the existence of a gradient within the root apex, with the highest CK concentration occurring in the lateral root cap, columella, columella initials, and QC cells. Relatively high CK concentration was also observed in the endodermis. Furthermore, the distribution of the majority of CK metabolites in GFP-expressing cell populations reveals their maxima in the apical part of the root tip. Finally, the total CK levels show the following progression among GFP-marked cell types: M0028:GFP > pSCR: GFP >> J2812:GFP > pWOL:GFP. This heterogeneous distribution of CKs in the Arabidopsis root apex indicates that there could either be a high rate of CK biosynthesis in these cell types and/or a high rate of transport into the cells.

Mapping the Cytokinin Metabolites in the Arabidopsis Root Apex

As summarized in Supplemental Figure 4C, total CK levels displayed variation between the GFP lines examined. Although six biological replicates were analyzed for each line, there may be variation due to genetic differences between the lines and/or
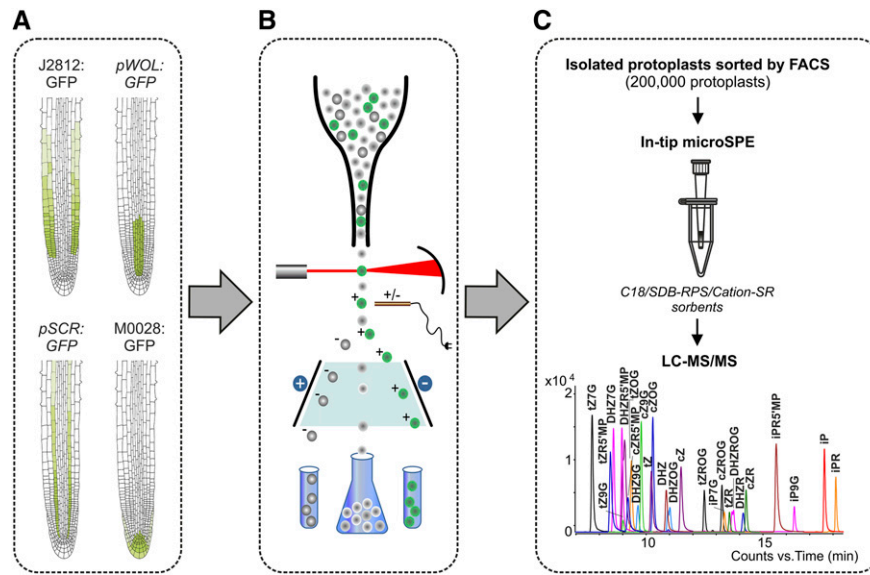
Figure 3. High-Resolution Cell-Specific Analysis of Cytokinin Distribution in the Arabidopsis Root Apex.

The methodology combined fluorescence-activated cell sorting of GFP-marked specific root tip cells with ultrasensitive mass spectrometry for the determination of 26 CK metabolites. Protoplasts were isolated from the roots of Arabidopsis seedlings (8 d after germination) expressing GFP in specific cell types **(A)** and then sorted using FACS **(B)**. The samples containing collected GFP-expressing (+, green) and non-GFP-expressing (–, gray) cell populations were purified by microSPE and analyzed by LC-MS/MS **(C)**.

technical variation since samples were each necessarily generated by cell sorting runs on different days. To compensate for these observed differences in CK concentrations between the transgenic lines, the CK content in each cell population is presented as the ratio of metabolite concentration between the GFP+ protoplasts and the internal reference GFP– population for each cell line (Figures 4 and 5). The GFP– population included non-GFP-expressing cells derived from the apical third of the root of each line; thus, the CKs quantified represent an average background level. In general, the CK metabolites showed similar trends in terms of their cell-specific distributions. Therefore, the data are also presented as a mean of total CK content (Figure 4B). However, the CK *O*-glucosides and nucleotides were not detected in the *pWOL:GFP* line, so information is lacking about these compounds in the stele cell population. The GFP+-to-GFP– ratios for each CK metabolite were also computed (Supplemental Figure 5). The *pSCR:GFP* and M0028:GFP lines showed statistically significant differences in their ratios compared with the J2812:GFP and *pWOL:GFP* lines (Figure 4B). Our data suggest that *pSCR:GFP* and M0028:GFP cells have lower and higher relative total CK content, respectively. Of the five CK metabolite groups, the pattern of CK bases, ribosides, and *N*-glucosides mirrored that of the total CK pool, while the GFP+-to-GFP– ratio of CK nucleotides in the J2812:GFP line was greatly lowered (Figure 4C). Summed levels of the three isoprenoid CK groups (*t*Z, *c*Z, and iP types) detected in the isolated protoplasts showed very similar patterns across the four Arabidopsis lines analyzed, with highest abundance in M0028:GFP cells (Figure 5B).

We next converted the mean of total CKs in each cell population into a CK level map for the root apex (Figure 5A). This type of visualization helps to understand the CK distribution across the four GFP-expressing lines, with clear evidence that

highest relative CK content was present in the M0028:GFP line. This line expresses GFP in the lateral root cap, columella, columella initials, and QC cells, in close agreement with the expression pattern of the synthetic CK reporter line, *TCSn:GFP* (Zürcher et al., 2013; Figure 5C). Moreover, individual distribution maps of each CK metabolite group (Supplemental Figure 6) show distinct patterns in the stele, the endodermis, the epidermis, and cortex cells. Together, these results strongly suggest the existence of CK gradients within the Arabidopsis root apex.

DISCUSSION

Cytokinin gradients within the root apex have already been predicted from promoter-reporter expression studies of CK-related genes. In Arabidopsis, the highest expression of a CK hydroxylase involved in biosynthesis of *trans*-zeatin (*CYP735A2*) is in the vasculature (Kiba et al., 2013) along with the cytokinin transporter (*ABCG14*) (Ko et al., 2014; Zhang et al., 2014), while cytokinin oxidase/dehydrogenase (*CKX4*) is expressed in the root cap. *CKX5* and *CKX6* expression is detected in the root vasculature with and without reaching the QC cells, respectively (Werner et al., 2003). However, because many CK compounds are mobile, CK-related gene expression analysis does not always represent the sites of hormone production, accumulation and biological function. We therefore decided to construct a CK distribution map based on direct measurements of CK pools in different cell types. In this detailed exploration of cell-specific cytokinin profiles, we were interested in all the different metabolic forms, including precursors, bioactive molecules, and inactivation products. Such data can lead to a better understanding of the CK content within distinct cell populations, tissues, and organs.
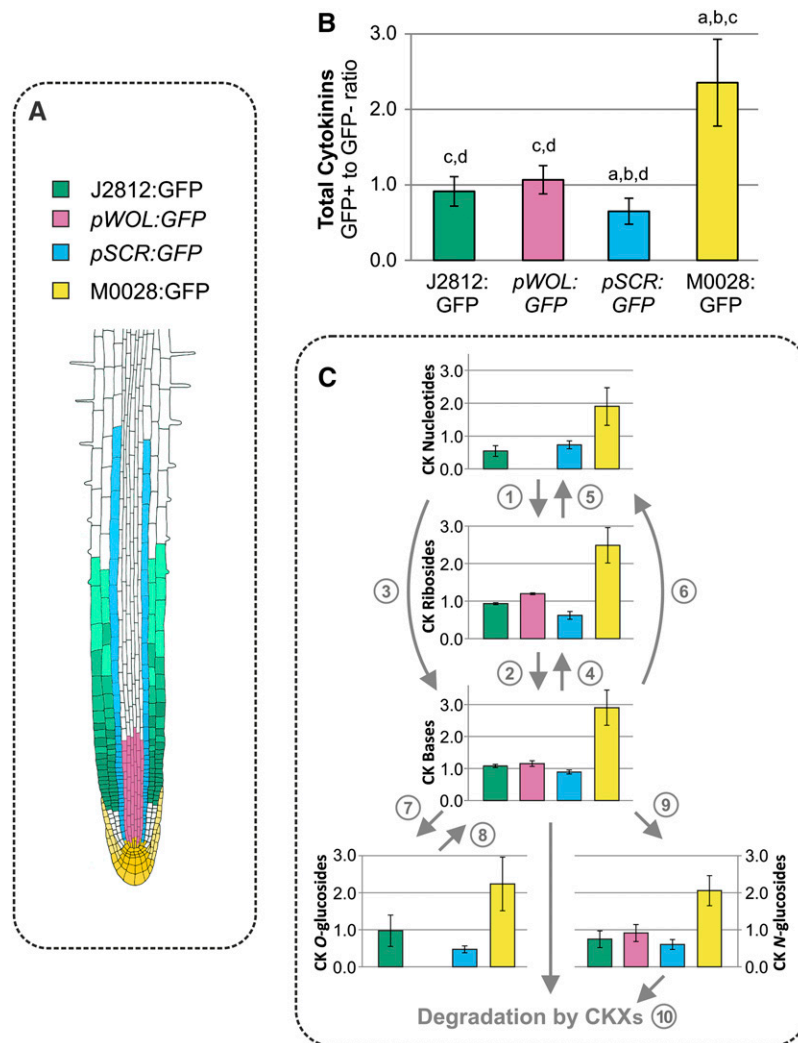
Figure 4. Cytokinin Levels in Four Different Cell Types Isolated from the Arabidopsis Root Apex.

(A) The localization of GFP expression in the root apex indicated in different colors for each Arabidopsis line expressing GFP in specific cell types.
(B) Total CK levels calculated as mean of the GFP+-to-GFP− ratio of all CK metabolites quantified. Letters above the bars are as follows: a, significantly different from J2812:GFP; b, significantly different from *pWOL:GFP*; c, significantly different from *pSCR:GFP*; d, significantly different from M0028:GFP (Student's *t* test, $P < 0.05$).
(C) Scheme of metabolism for different cytokinin metabolite groups. The metabolic pathways are based on Spíchal (2012). Enzymes involved in CK biosynthesis, interconversions, and degradation are indicated by circled numbers: (1) 5′-ribonucleotide phosphohydrolase, (2) adenosine nucleosidase, (3) CK phosphoribohydrolase 'Lonely Guy', (4) purine nucleoside phosphorylase, (5) adenosine kinase, (6) adenine phosphoribosyltransferase, (7) zeatin-*O*-glucosyltransferase, (8) β-glucosidase, (9) *N*-glucosyl transferase, and (10) CKX.
The CK metabolites were quantified in fmol/100,000 isolated protoplasts, and the GFP+-to-GFP− ratios were computed for each sorted transgenic line: J2812:GFP, *pWOL:GFP*, *pSCR:GFP*, and M0028:GFP. In the *pWOL:GFP* line, CK *O*-glucosides and nucleotides were detected in neither the GFP+ nor the GFP− cell populations. Data represent six biological replicates, and for each, two technical replicates were performed. Error bars indicate SE.

To unravel the pattern of CK metabolites within individual cell types of the Arabidopsis root apex, the newly developed method combining FACS and UHPLC-MS/MS was used to quantify CKs in four spatially distinct GFP-expressing cell populations within the root tip (Figure 3), enabling generation of a detailed cell map of CK distribution in the Arabidopsis root apex (Figure 4A). The approach followed was previously applied to develop equivalent maps of auxin distribution (Petersson et al., 2009; Pĕnčík et al., 2013). However, the presence of CKs in plant tissues at extremely low concentrations (pmol·g^{-1} fresh weight), ~100-fold lower than auxin concentration, makes their quantification from very small samples highly challenging. Improvements in mass spectrometry during the last 15 years made it possible now to identify and quantify CKs from milligram quantities of plant tissues (Svačinová et al., 2012). The optimized methodology shown in Figure 3 enabled the performance of cell-type-specific quantification of CK metabolites in transgenic lines with GFP expression in less than 50 cells per root tip (M0028:GFP line; Swarup et al., 2005).
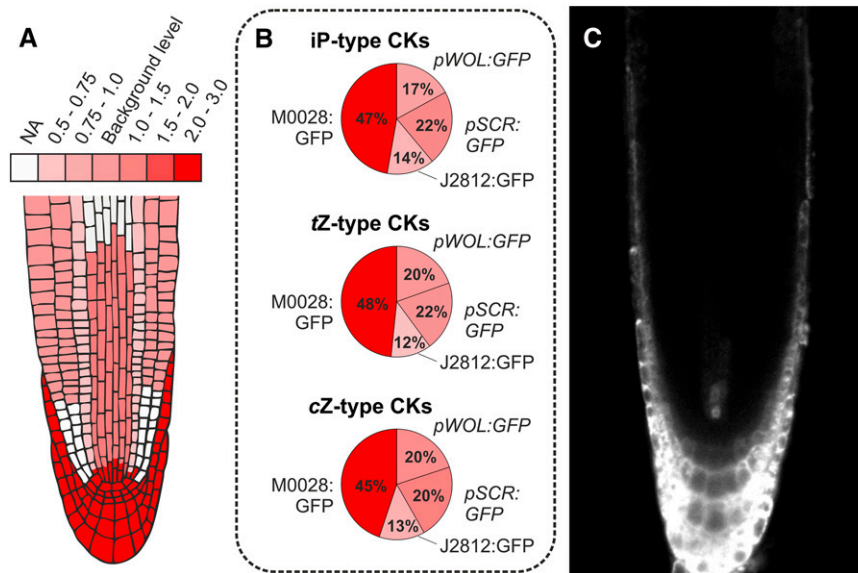
Figure 5. Cytokinin Distribution within the Arabidopsis Root Tip.

(A) CK gradient map showing a concentration maximum in the lateral root cap, columella, columella initials, and QC cells.

(B) CK distribution of three isoprenoid groups (*tZ*, *cZ*, and iP types) detected in isolated protoplasts.

(C) *TCSn:GFP* expression pattern in 5-d-old Arabidopsis root tip.

The data presented in the map were derived from four GFP lines (J2812:GFP, *pWOL:GFP*, *pSCR:GFP*, and M0028:GFP) covering almost all of the different cell types of the root apex. Cell-type-specific CK concentrations were calculated in fmol/100,000 isolated GFP⁺ protoplasts and then normalized to the GFP⁻ reference population for each GFP cell line. The red color scale indicates the CK content relative to this reference population; NA represents cell populations that were not analyzed. A value of 1 represents CK level in GFP⁺ cells equivalent to that in reference GFP⁻ cells.

The so-called StageTip (Stop and Go Extraction Tip) technology, which has been developed for desalting, micropurification, enrichment, and prefractionation of proteins and peptides prior to LC-MS analysis (Rappsilber et al., 2003, 2007; Ishihama et al., 2006) was recently adapted for isolation and quantification of CKs in minute amounts of fresh plant tissues (1 to 5 mg) using a combination of two reverse phases [C_{18} and poly(styrene-divinylbenzene) copolymer modified with sulfonic acid groups (SDB-RPS)] and one cation-exchange phase (Cation-SR) (Svačinová et al., 2012). A similar microSPE protocol (Supplemental Figure 2) was successfully optimized to enable the rapid and effective extraction and purification of CKs from a minimal quantity of protoplasts, with efficient isolation and enrichment (Supplemental Figure 1). This was coupled with a faster, highly selective and extremely sensitive UHPLC-MS/MS analysis (Supplemental Table 1) to facilitate the screening of 26 isoprenoid CK metabolites in specific Arabidopsis root cell populations (Supplemental Figure 4C). It has previously been published that the average cell diameters of the four different cell populations of the Arabidopsis root apex examined here were not significantly different (Petersson et al., 2009), allowing comparisons of the CK levels among the individual cell types. CK concentration of the GFP⁺ protoplasts was then normalized to the concentration of the respective GFP⁻ protoplasts, in order to compensate for changes in CK levels caused by slight differences in growth conditions and genetic background.

Importantly, the method was tested for alterations in CK metabolism and content, and for leakage of CKs from protoplasts, during the protoplast isolation and cell sorting procedures,

respectively. As displayed in Figure 1A, inhibiting CK degradation with the specific CKX inhibitor, INCYDE, resulted in slightly elevated levels of the CK bases iP and *tZ* and the riboside iPR, compounds known to be efficiently degraded by CKXs (Gajdosová et al., 2011; Köllmer et al., 2014). Treatment with adenine (Figure 1B), a known cytokinin transport antagonist (Bürkle et al., 2003; Cedzich et al., 2008), caused a slight decrease of *cZ* and *tZ* bases and increased levels of their respective ribosides. This is in accordance with the H⁺-coupled high-affinity purine uptake transporter system shared by the structurally similar CK bases and adenine. Likewise, CK transport competition studies showed that there was a stronger inhibition of labeled adenine uptake when competing with *tZ* than with zeatin riboside (Bürkle et al., 2003). Inhibition of ATP-dependent metabolic and membrane transport processes (Tucker, 1993) with **s**odium azide also resulted in less than 2-fold changes in CK metabolite concentrations (Figure 1C). In addition to inhibition of respiration (Drake 1979), **s**odium azide also causes other changes in plant cells, including increased cytosolic Ca^{2+} levels (Gilroy et al., 1989) and reduction of intracellular pH (Spanswick and Miller, 1977). The latter might have an impact, for example, on CKX enzyme activity, which is highly pH dependent (Galuszka et al., 2007) and thus could alter CK metabolism. Taken together, the data derived from these chemical treatments suggest that during protoplast isolation, CK metabolism is still active but at sufficiently low levels to allow estimation of endogenous CK concentrations. Further evidence of the robustness and reproducibility of the methods comes from examination of CK leakage from the isolated protoplasts during cell sorting

(Figure 2). CK content of the protoplast pellets changed only slightly during the 3-h period required for sorting at 4°C, while no significant leakage was detected over this period. The CKs detected in the supernatant samples (Figure 2B) instead may derive from damaged protoplasts and undigested cell wall fragments accumulated during protoplast isolation.

The four transgenic Arabidopsis lines, described in Figure 3A, were chosen due to the distribution of their tissue-specific fluorescent labeling collectively covering all cell types within the root apex. Using the method developed here, it can now be estimated that the concentration of CK metabolites in a single root cell is in the zeptomole range (between 3×10^{-21} and 100×10^{-21} mol per cell). This is somewhat lower than previous estimations of total CK levels in potato (*Solanum tuberosum*) shoot meristematic cells (600×10^{-21} to 5000×10^{-21} mol per cell) (Turnbull and Hanke, 1985). It should be also taken into account that only intracellular CKs were quantified using this method since the measurements derived from protoplast samples. However, since CK receptors have been shown to be localized in the endoplasmic reticulum (Caesar et al., 2011; Wulfetange et al., 2011; Lomin et al., 2012), intracellular CKs can be considered of crucial importance. Indeed, the active CK bases displayed enriched levels in the endodermis, whereas CK nucleotides were at similar levels in this cell type. This could indicate CK biosynthesis in the endodermis and possible direct conversion to the CK bases. Conversion of the bioactive forms back to their phosphate precursor forms also cannot be excluded.

Most of the iP-, *tZ*-, and *cZ*-type CKs were consistently detected in all the root cell types investigated (Supplemental Figure 3). Interestingly, it was shown that *cZ*-type CKs were the predominant forms in Arabidopsis root apices followed by iP types, whereas *tZ*-type CKs were detected at much lower levels than the other forms (Figure 2; Supplemental Figure 4C). These findings are in agreement with previous evidence that *cZ*-type CKs are enriched in the apical part of the Arabidopsis root. Bielach et al. (2012) measured CK concentration in root segments representing zones of lateral root initiation, lateral root formation, and lateral root emergence and showed that *cZ* and *cZR* concentration increased significantly from lateral root emergence to lateral root initiation zones. Consistently, *tZRMP* and *tZR* levels were below the detection limit in the root tip. This could be explained by the constrained local expression of *CYP735A2* in only a few columella cells compared with the main expression site of the gene in the root vasculature (Kiba et al., 2013). However, *tZ* was present in all cell types examined. We therefore hypothesize that *tZRMP* is produced in the *CYP735A2*-expressing columella cells, which is converted with a high efficiency to *tZ* through *LOG* gene activity and then transported through ABCG14 (Ko et al., 2014; Zhang et al., 2014) to the other cell types of the root tip. In broader terms, the lack of detection of *tZRMP* and *tZR* is consistent with the reduced levels of all *tZ*-type forms detected in the root tip (*tZ*, *tZ7G*, *tZ9G*, and *tZOG*) compared with levels of iP and *cZ* types (Supplemental Figure 4C). Our results further show that the CK metabolite pattern in each transgenic line examined was highly similar between GFP-expressing and non-GFP-expressing cells (Supplemental Figure 3). In accordance with this, concentration of all CK types detected (grouped as iP, *tZ*, and *cZ* metabolites) displayed almost the same distribution pattern in all other cell populations of the Arabidopsis root apex (Supplemental Figure

4C). Taken together, these findings indicate that CK enrichment in specific cell types is not compound or CK type specific and thus represents total CK concentration levels.

A series of cell-type-specific CK maps of the Arabidopsis root apex was constructed for total CKs and for each of the CK metabolite groups (Figure 5A; Supplemental Figure 6). These maps all strongly suggest that there is a gradient of CKs in the apical part of the Arabidopsis primary root with a maximum in the lateral root cap, columella, columella initials, and QC cells. This was confirmed from both our quantitative analysis of the data (Supplemental Figure 4A) and the normalized data using the respective GFP⁻ cells as a reference cell population for each line (Figure 5A). As shown also in Figure 5C, CK enrichment in the lateral root cap, columella, columella initials, and QC cells is in accordance with the expression patterns of *TCSn:GFP*, a widely used CK reporter line (Zürcher et al., 2013). In previous studies, exogenous CK application reduced the root meristem size, consistent with enlarged meristems displayed by the triple *ipt3,5,7* CK biosynthesis mutant (Dello Ioio et al., 2007). In the same work, it was further shown that the CK depletion required for delimiting the meristem was spatially restricted to the transition zone. Likewise, our results show no CK maxima in the J2812:GFP and *pSCR:GFP* cell populations that extend into the transition zone.

The free bases iP, *cZ*, and *tZ* are the most active CKs and showed greatest accumulation in the columella, lateral root cap, columella initials, and QC cell populations (Figure 4; Supplemental Figure 6). The same trend was seen for their corresponding precursor and conjugate forms, suggesting local metabolism and turnover. The *tZ* content in these cell types was the highest among the free bases, whereas iP showed relatively enhanced content also in the stele (Supplemental Figure 5). The latter trend matches the maximal expression of the *ARABIDOPSIS HISTIDINE KINASE4* (*AHK4*) receptor gene in the vascular initials (Nishimura et al., 2004) and is consistent with AHK4 having significantly higher affinity than AHK3 for iP compared with *tZ* in both Arabidopsis and maize (*Zea mays*) (Yonekura-Sakakibara et al., 2004; Romanov et al., 2006).

A complementary cell-specific analysis of the Arabidopsis root apex compiled the expression data for 107 CK-related genes (Supplemental Tables 2 and 3). The data were derived from four individual microarray and proteomic studies in distinctive cell populations of the root (Birnbaum et al., 2003; Brady et al., 2007; Dinneny et al., 2008; Petricka et al., 2012). To compare the cell-specific gene expression of CK-related genes with the CK gradient maps (Figure 5; Supplemental Figure 6), the data were classified into four categories corresponding to the cell-type populations in which M0028:GFP, J2812:GFP, *pWOL:GFP*, and *pSCR:GFP* are expressed. The data set (Supplemental Table 3) was then augmented by multiple studies of promoter driven CK-related expression of *GUS* and/or *GFP* reporters (Werner et al., 2003; Miyawaki et al., 2004; Mähönen et al., 2006; Kuroha et al., 2009; Kiba et al., 2013; Zürcher et al., 2013; Zhang et al., 2014).

This cell-specific meta-analysis of the Arabidopsis root apex indicated that out of the 12 CK-related genes enriched in the cell types of lateral root cap, columella, columella initials, and QC cells (M0028:GFP) where the CK maximum was determined, two belonged to the *CKX* family and another two to the *URIDINE DIPHOSPHATE GLUCOSYLTRANSFERASE* (*UGT*) family. Both these enzymes deactivate CKs. These findings are in agreement
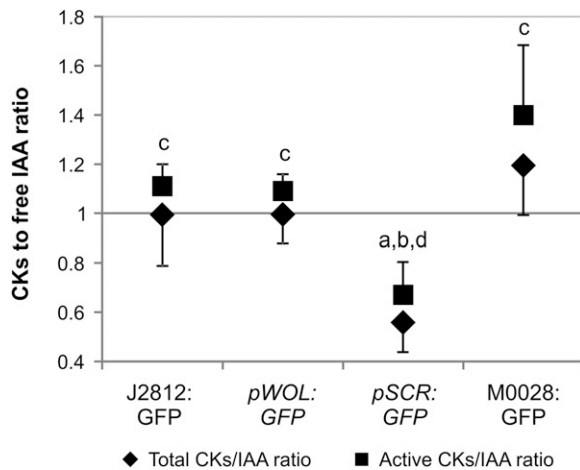
Figure 6. Ratio of Cytokinins to Free IAA in Four Different GFP-Expressing Cell Populations.

Ratio between the relative content of CKs and free IAA (diamonds, total CKs/IAA; squares, active CKs/IAA) in four Arabidopsis lines (M0028:GFP, *pWOL:GFP*, *pSCR:GFP*, and J2812:GFP) expressing GFP protein. Active CK forms represent sum of CK bases and ribosides; total CKs represent sum of all CK metabolites detected. The concentrations of free IAA were analyzed in same sorted cell populations using LC-MS/MS (published in Pěnčík et al., 2013). Prior to the final CK/IAA ratio computing, the data for both hormones had been normalized against the concentration of their respective internal reference population, consisting of the non-GFP-expressing cells from the same samples. Error bars indicate SE ($n = 6$). Both ratios of CKs to free IAA showed similar statistical patterns; letters above the bars are as follows: a, significantly different from J2812:GFP; b, significantly different from *pWOL:GFP*; c, significantly different from *pSCR:GFP*; d, significantly different from M0028:GFP (Student's *t* test, P < 0.05).

with previous evidence that enhanced *CKX* activity corresponds to high concentrations of CKs (Motyka et al., 1996; Gaudinová et al., 2005) and that the *ugt76c2* mutant has reduced levels of most CK metabolites (Wang et al., 2013). In Supplemental Figure 6, it is also shown that the CK content in the respective gradient maps differs according to the CK metabolite group. Although CK bases are often considered the main bioactive forms, we grouped the bases and ribosides together because they both have high activities in CK receptor in vitro assays and in bioassays (Spíchal et al., 2004; Romanov et al., 2006). These CKs displayed the highest content in the root tip followed by cytokinin *N*- and *O*-glucosyl conjugates, with the nucleotide precursors being the least abundant CK forms. This profile is in accordance with the CK gene expression gradients presented in Supplemental Table 3. Expression of several *LOG* genes, which catalyze the conversion from nucleotides to CK bases, and gene families linked with CK signaling (ARRs and CRFs) were enriched in all the cell types examined. Enhanced transcript levels of *UGT* genes encoding for CK glucosyltransferases were also present in all the cell populations apart from endodermis. Finally, genes responsible for CK nucleotide biosynthesis showed the least abundant expression: Expression of *IPT* and *CYP73A2* genes was enriched in the stele and in the columella, respectively. These complementary profiles between CK gene expression and metabolite abundance reinforce our evidence for the presence of a CK gradient in the Arabidopsis root apex.

Cytokinin response profiles have previously been reported to complement the corresponding profile of auxin in Arabidopsis root apex. While expression of the auxin signaling reporter DR5 was maximal in the central columella cells, the *TCSn*-monitored CK output exhibited its highest enrichment in the outer columella cells surrounding the *DR5* territory (Bielach et al., 2012). Asymmetric distributions of auxin and cytokinin in the root tip are suggested to be needed for gravitropic response to facilitate downward root bending (Aloni et al., 2006). We therefore compared our CK distribution map of the Arabidopsis root apex with the corresponding data for auxin derived from the same transgenic lines (Pěnčík et al., 2013). The ratios of the contents of total CKs:IAA and active CKs:IAA were then calculated (Figure 6). Both ratios showed that in the epidermis, cortex, and stele cells, the relative content of the two hormones is quite similar, whereas in the endodermis, the IAA level is significantly elevated relative to that of CKs. In contrast, relative CK content is slightly higher than IAA in the cell population containing columella, lateral root cap, columella initials, and QC. The antagonistic interactions of these two major hormone groups within the root tissues regulating several critical aspects of development and organogenesis have been reported many times, specifically in root apical meristem size determination (Dello Ioio et al., 2007, 2008), embryonic root stem cell niche specification (Müller and Sheen, 2008), determination of QC activity (Zhang et al., 2013), root vasculature patterning (Bishopp et al., 2011), and lateral root primordia formation (Moreira et al., 2013). As recently reviewed by Schaller et al. (2015), in all the above-mentioned functions regulated by auxin and cytokinin interplay, there are spatially bisymmetric response maxima of the two hormones. However, this information derives only from reporter lines for each of the two hormone signaling pathways. The CK map generated here, combined with the respective work for auxin (Petersson et al., 2009), enables direct measurement of levels of the two hormones at these cellular sites of action. Based on the hormone ratios estimated in Figure 6, it can be predicted that auxin and CK interactions may vary depending on the cell type within the Arabidopsis root tip.

Here, we established tools for cell-specific quantification of CKs within the Arabidopsis root apex. The selectivity of FACS in combination with sensitivity of mass spectrometry measurements have great potential to provide a deeper understanding of CK biosynthesis and regulation of homeostasis at the cellular level. The combination of such knowledge about the cytokinin-auxin hormonal interplay can shed light on complex regulatory aspects of plant development.

METHODS

Cell-Specific Analysis of the *Arabidopsis thaliana* Root Apex

Root protoplasts were isolated from four different lines expressing GFP in specific cell types of the root apex. GFP+ and GFP− protoplasts were isolated through FACS, purified by multilayer microSPE, and analyzed for cytokinin content by ultra-high-sensitivity mass spectrometry, as described below. The detection of the hormone in such minute amounts as 50,000 to 200,000 cells was achieved by high optimization of all parts of the method prior to the analysis of the samples.

Plant Material and Growth Conditions

Four well-characterized GFP-expressing lines (shown in Figure 3A) were selected to cover all cell types in the Arabidopsis root apex (epidermis, cortex, stele, endodermis, lateral root cap, columella, columella initials, and QC); *pWOODEN LEG:GFP* (*pWOL:GFP*) and *pSCARECROW:GFP* (*pSCR:GFP*) are in the Columbia genetic background (Birnbaum et al., 2003), while the M0028:GFP (Swarup et al., 2005) and J2812:GFP lines are in the C24 background and derive from the Haseloff GAL4-GFP enhancer trap collections (Haseloff Lab, University of Cambridge). Col-0 wild-type seedlings were used for the control experiments. All seeds were sterilized using 20% (v/v) bleach and 0.1% Tween for 5 min (2 × 2.5 min) and then rinsed five times with sterile water. They were then sown in three rows (~100 seeds/row) on square Petri dishes containing standard Murashige and Skoog medium (1× concentration Murashige and Skoog salt mixture: 4.4 g/L, 1% sucrose, 0.5 g/L MES, 1% agar and adjusted to pH 5.7 with KOH) covered with sterile mesh squares to facilitate the harvesting of the apical part of the primary root. All plated seeds were stratified for 3 d in darkness at 4°C before being transferred to 23°C and long-day conditions (16 h light and 8 h darkness) where they were grown vertically for 8 d (under 150 μmol m^{-2} s^{-1} light). One standard cell-sorting experiment required 30 to 40 Petri dishes. For confocal microscopy experiments, seeds of the *TCSn:GFP* line (Zürcher et al., 2013) were also sterilized, sown (~10 seeds/row), and grown for 5 d as described above.

Protoplast Isolation

The apical parts of the seedling roots (approximately one-third of the root) were harvested and rinsed with distilled water. The collected root part was then further dissected in 2- to 5-mm pieces and added to 100-mL flasks containing 25 mL protoplast isolation buffer (600 mM mannitol, 2 mM MgCl$_2$, 10 mM KCl, 2 mM CaCl$_2$, 2 mM MES, and 0.1% BSA, pH 5.7) containing cell wall disintegrating enzymes (0.3 units/mL pectolyase and 45 units/mL cellulysin). The solution was incubated for 2 h at 22°C in darkness and with stirring at 125 rpm (manual stirring also occurred every 20 min). The incubation of all individual biological replicates took place between 9 and 11 AM to avoid any circadian clock effect. The protoplasts were separated from the undigested root tissue using a 40-μm cell filter (Becton Dickinson and Company) and centrifuged for 3 min at 1000 relative centrifugal force (Hettich Universal 32) at 4°C. The resulting protoplast pellet was resuspended in 1 mL of sorting buffer (0.7% NaCl) and kept at 4°C until initiation of cell sorting.

Cell Sorting

In order to separate the GFP$^+$ from the GFP$^-$ root protoplasts of each GFP-expressing line, cell sorting was performed using a BD FACS Aria I flow cytometer (BD Biosciences) as described by Petersson et al. (2009) and Pěnčík et al. (2013) with minor modifications. The resuspended isolated protoplasts were loaded in the cell sorter (4°C) and passed individually through a 100-μm nozzle (Becton Dickinson and Company) using 0.7% NaCl as sorting buffer. The undamaged protoplasts were selected according to their forward and side scatter light absorption, while the fluorescent ones were distinguished by their GFP excitation (488-nm laser) using their autofluorescence as a control. The isolated cell populations were frozen immediately after sorting with liquid nitrogen and stored at −80°C until purification. The software used for data processing was BD FACSDiva version 6.1.2.

Cytokinin Purification Protocols

Aliquots of around 200,000 protoplasts in 0.7% NaCl (~1 mL) were diluted with water at a ratio of 3:1 (v/v) and adjusted to pH 2.7 with 1 M HCl. Prior to extraction, 0.1 to 1.0 pmol of isotope-labeled CK standards (Olchemim) were added to each sample as follows: 0.1 pmol of [^{13}C$_5$]cZ, [^{13}C$_5$]tZ, [^{2}H$_3$] dihydrozeatin (DHZ), [^{2}H$_6$]iP, [^{2}H$_5$]tZR, [^{2}H$_3$]DHZR, [^{2}H$_6$]iPR, [^{2}H$_5$]tZ7G, and

[^{2}H$_6$]iP7G; 0.2 pmol of [^{2}H$_5$]tZOG, [^{2}H$_7$]DHZOG, [^{2}H$_5$]tZ9G, [^{2}H$_3$]DHZ9G, and [^{2}H$_6$]iP9G; 1.0 pmol of [^{2}H$_5$]tZROG, [^{2}H$_5$]tZRMP, [^{2}H$_3$]DHZRMP, and [^{2}H$_6$]iPRMP. Two SPE protocols were tested according to previously published purification methods with some modifications (Dobrev and Kamínek, 2002; Svačinová et al., 2012). The first method used Oasis MCX cartridges (1 mL/30 mg; Waters) conditioned with 1 mL each of 100% methanol and water, equilibrated sequentially with 1 mL of 50% (v/v) nitric acid, 1 mL of water, and 1 mL of 1 M HCOOH. After sample application onto an Oasis MCX column, unretained compounds were removed by a wash step using 1 mL of 1 M HCOOH and preconcentrated analytes were eluted by two-step elution using 1 mL of 0.35 M NH$_4$OH aqueous solution and 2 mL of 0.35 M NH$_4$OH in 60% (v/v) methanol solution. The second method utilized the in-tip microSPE based on the StageTips technology (Rappsilber et al., 2003). The final optimized microSPE protocol is shown in Supplemental Figure 2. Briefly, combined multi-StageTips (containing C$_{18}$/SDB-RPSS/Cation-SR layers) were activated sequentially with 50 μL each of acetone, methanol, water, 50% (v/v) nitric acid, and water (by centrifugation at 2000 rpm, 15 min, 4°C). After application of the sample (200 μL, 2500 rpm, 30 min, 4°C), the microcolumns were washed sequentially with 50 μL of water and methanol (2200 rpm, 20 min, 4°C), and elution of samples was performed with 50 μL of 0.5 M NH$_4$OH in 60% (v/v) methanol (2200 rpm, 20 min, 4°C). Eluates were evaporated to dryness using a SpeedVac concentrator and dissolved in 40 μL of 10% methanol. Ten microliters of each sample was then analyzed using UHPLC-MS/MS.

UHPLC-MS/MS Method

Separation and determination of samples were performed on a 1290 Infinity Binary LC System coupled to the 6490 Triple Quad LC/MS System with Jet Stream and Dual Ion Funnel technologies in positive mode (Agilent Technologies). The samples were injected onto a reverse-phase column (Acquity UPLC CSH C18 1.7 μm, 2.1 × 150 mm; Waters) and separated using a gradient of methanol (A) and 15 mM ammonium formate (pH 3.95, B) at a flow rate of 0.35 mL·min^{-1}. The gradient used was: 0 min, 10:90 (A:B) to 10.0 min, 23:77 (A:B) to 15.0 min, 36:64 (A:B). At the end of the gradient, the column was washed with 100% methanol and reequilibrated to initial conditions (5 min). Column temperature was set to 45°C and sample temperature to 4°C. Determination of endogenous CKs in protoplasts was performed by multiple reaction monitoring of the protonated precursor and appropriate product ions. The multiple reaction monitoring transitions, optimized instrument settings, retention times, and detection limits are shown in Supplemental Table 1. MassHunter software (version B.05.02; Agilent Technologies) was used to determine the concentrations of CKs using stable isotope dilution.

Control Experiments

Protoplast Treatments

Root protoplasts were isolated as described above from Col-0 wild-type roots while being simultaneously treated with either 10 μM INCYDE (Zatloukal et al., 2008), 100 μM adenine, 3 mM NaN$_3$, or the DMSO control, by adding the chemicals into the protoplast isolation buffer. The isolated protoplasts were collected by centrifugation and resuspended in 200 μL of sorting buffer. The CKs were purified through MCX columns and their content was measured as previously described.

Leakage Tests

Isolated root protoplasts from Col-0 wild-type roots were resuspended in 1 mL of cold sorting buffer and kept on ice for 180 min, imitating the sorting procedure. After 0, 90, or 180 min, protoplast samples were centrifuged for 3 min at 1000 rpm at 4°C. The pellet and respective supernatant were separated and processed for CK quantification.

Confocal Microscopy

GFP expression patterns in 5-d-old seedlings of the transgenic Arabidopsis line *TCSn:GFP* were recorded using confocal laser scanning microscopy (Zeiss LSM 780). Contrast adjustments were performed using ImageJ (http://imagej.nih.gov/ij/).

Accession Numbers

The accession numbers of all 107 cytokinin-related genes examined by complementary cell-specific analysis of the Arabidopsis root apex can be found in Supplemental Table 2.

Supplemental Data

Supplemental Figure 1. Recovery (%) of different cytokinin groups in relation to the number of sorbent multilayers (C_{18}/SDB-RPS/Cation-SR) and total process efficiency (%) of in-tip microSPE protocol.

Supplemental Figure 2. Optimized in-tip microSPE protocol.

Supplemental Figure 3. Cytokinin metabolite patterns in GFP-expressing and GFP-nonexpressing cells of four transgenic Arabidopsis lines.

Supplemental Figure 4. Cytokinin concentration gradient exists within the Arabidopsis root apex.

Supplemental Figure 5. Cytokinin metabolism in four different GFP-expressing cell populations.

Supplemental Figure 6. Distribution of cytokinin metabolite groups within the Arabidopsis root tip.

Supplemental Table 1. MS optimized conditions.

Supplemental Table 2. List of 107 cytokinin-related genes indicated with their published name and their corresponding accession number.

Supplemental Table 3. Cytokinin-related gene expression enriched in *pWOL:GFP*, M0028:GFP, *pSCR:GFP*, and J2812:GFP cell types.

AUTHOR CONTRIBUTIONS

O.N., K.L., C.T., and K.D. designed the research. I.A., L.P., B.S., and O.N. performed the research, contributed new analytical tools, and analyzed data. O.N., I.A., K.L., L.P., K.D., and C.T. wrote the article.

REFERENCES

Aloni, R., Aloni, E., Langhans, M., and Ullrich, C.I. (2006). Role of cytokinin and auxin in shaping root architecture: regulating vascular differentiation, lateral root initiation, root apical dominance and root gravitropism. Ann. Bot. (Lond.) **97:** 883–893.

Aremu, A.O., Bairu, M.W., Novák, O., Plačková, L., Zatloukal, M., Doležal, K., Finnie, J.F., Strnad, M., and Van Staden, J. (2012). Physiological responses and endogenous cytokinin profiles of tissue-cultured 'Williams' bananas in relation to roscovitine and an inhibitor of cytokinin oxidase/dehydrogenase (INCYDE) treatments. Planta **236:** 1775–1790.

Bielach, A., Podlesáková, K., Marhavy, P., Duclercq, J., Cuesta, C., Müller, B., Grunewald, W., Tarkowski, P., and Benková, E. (2012). Spatiotemporal regulation of lateral root organogenesis in *Arabidopsis* by cytokinin. Plant Cell **24:** 3967–3981.

Birnbaum, K., Jung, J.W., Wang, J.Y., Lambert, G.M., Hirst, J.A., Galbraith, D.W., and Benfey, P.N. (2005). Cell type-specific expression profiling in plants via cell sorting of protoplasts from fluorescent reporter lines. Nat. Methods **2:** 615–619.

Birnbaum, K., Shasha, D.E., Wang, J.Y., Jung, J.W., Lambert, G.M., Galbraith, D.W., and Benfey, P.N. (2003). A gene expression map of the *Arabidopsis* root. Science **302:** 1956–1960.

Bishopp, A., Help, H., El-Showk, S., Weijers, D., Scheres, B., Friml, J., Benková, E., Mähönen, A.P., and Helariutta, Y. (2011). A mutually inhibitory interaction between auxin and cytokinin specifies vascular pattern in roots. Curr. Biol. **21:** 917–926.

Brady, S.M., Orlando, D.A., Lee, J.Y., Wang, J.Y., Koch, J., Dinneny, J.R., Mace, D., Ohler, U., and Benfey, P.N. (2007). A high-resolution root spatiotemporal map reveals dominant expression patterns. Science **318:** 801–806.

Bürkle, L., Cedzich, A., Döpke, C., Stransky, H., Okumoto, S., Gillissen, B., Kühn, C., and Frommer, W.B. (2003). Transport of cytokinins mediated by purine transporters of the PUP family expressed in phloem, hydathodes, and pollen of *Arabidopsis*. Plant J. **34:** 13–26.

Caesar, K., Thamm, A.M., Witthöft, J., Elgass, K., Huppenberger, P., Grefen, C., Horak, J., and Harter, K. (2011). Evidence for the localization of the Arabidopsis cytokinin receptors AHK3 and AHK4 in the endoplasmic reticulum. J. Exp. Bot. **62:** 5571–5580.

Cedzich, A., Stransky, H., Schulz, B., and Frommer, W.B. (2008). Characterization of cytokinin and adenine transport in *Arabidopsis* cell cultures. Plant Physiol. **148:** 1857–1867.

Dello Ioio, R., Linhares, F.S., Scacchi, E., Casamitjana-Martinez, E., Heidstra, R., Costantino, P., and Sabatini, S. (2007). Cytokinins determine *Arabidopsis* root-meristem size by controlling cell differentiation. Curr. Biol. **17:** 678–682.

Dello Ioio, R., Nakamura, K., Moubayidin, L., Perilli, S., Taniguchi, M., Morita, M.T., Aoyama, T., Costantino, P., and Sabatini, S. (2008). A genetic framework for the control of cell division and differentiation in the root meristem. Science **322:** 1380–1384.

Dinneny, J.R., Long, T.A., Wang, J.Y., Jung, J.W., Mace, D., Pointer, S., Barron, C., Brady, S.M., Schiefelbein, J., and Benfey, P.N. (2008). Cell identity mediates the response of *Arabidopsis* roots to abiotic stress. Science **320:** 942–945.

Dobrev, P.I., and Kamínek, M. (2002). Fast and efficient separation of cytokinins from auxin and abscisic acid and their purification using mixed-mode solid-phase extraction. J. Chromatogr. A **950:** 21–29.

Drake, G.A. (1979). Electrical coupling, potentials, and resistances in oat coleoptiles: effects of azide and cyanide. J. Exp. Bot. **30:** 719–725.

El-Showk, S., Ruonala, R., and Helariutta, Y. (2013). Crossing paths: cytokinin signalling and crosstalk. Development **140:** 1373–1383.

Gajdosová, S., et al. (2011). Distribution, biological activities, metabolism, and the conceivable function of cis-zeatin-type cytokinins in plants. J. Exp. Bot. **62:** 2827–2840.

Galuszka, P., Popelková, H., Werner, T., Frébortová, J., Pospíšilová, H., Mik, V., Köllmer, I., Schmülling, T., and Frébort, I. (2007). Biochemical characterization of cytokinin oxidases/dehydrogenases from *Arabidopsis thaliana* expressed in *Nicotiana tabacum* L. J. Plant Growth Regul. **26:** 255–267.

Gaudinová, A., Dobrev, P.I., Šolcová, B., Novák, O., Strnad, M., Friedecký, D., and Motyka, V. (2005). The involvement of cytokinin oxidase/dehydrogenase and zeatin reductase in regulation of cytokinin levels in pea (*Pisum sativum* L.) leaves. J. Plant Growth Regul. **24:** 188–200.

Gilroy, S., Hughes, W.A., and Trewavas, A.J. (1989). A comparison between quin-2 and aequorin as indicators of cytoplasmic calcium levels in higher plant cell protoplasts. Plant Physiol. **90:** 482–491.

Hirose, N., Makita, N., Yamaya, T., and Sakakibara, H. (2005). Functional characterization and expression analysis of a gene, OsENT2, encoding an equilibrative nucleoside transporter in rice suggest a function in cytokinin transport. Plant Physiol. **138:** 196–206.

Ishihama, Y., Rappsilber, J., and Mann, M. (2006). Modular stop and go extraction tips with stacked disks for parallel and multidimensional peptide fractionation in proteomics. J. Proteome Res. **5:** 988–994.

Jones, B., Gunnerås, S.A., Petersson, S.V., Tarkowski, P., Graham, N., May, S., Doležal, K., Sandberg, G., and Ljung, K. (2010). Cytokinin regulation of auxin synthesis in *Arabidopsis* involves a homeostatic feedback loop regulated via auxin and cytokinin signal transduction. Plant Cell **22:** 2956–2969.

Kiba, T., Takei, K., Kojima, M., and Sakakibara, H. (2013). Side-chain modification of cytokinins controls shoot growth in *Arabidopsis.* Dev. Cell **27:** 452–461.

Ko, D., et al. (2014). *Arabidopsis* ABCG14 is essential for the root-to-shoot translocation of cytokinin. Proc. Natl. Acad. Sci. USA **111:** 7150–7155.

Köllmer, I., Novák, O., Strnad, M., Schmülling, T., and Werner, T. (2014). Overexpression of the cytosolic cytokinin oxidase/dehydrogenase (CKX7) from *Arabidopsis* causes specific changes in root growth and xylem differentiation. Plant J. **78:** 359–371.

Kuroha, T., Tokunaga, H., Kojima, M., Ueda, N., Ishida, T., Nagawa, S., Fukuda, H., Sugimoto, K., and Sakakibara, H. (2009). Functional analyses of LONELY GUY cytokinin-activating enzymes reveal the importance of the direct activation pathway in *Arabidopsis.* Plant Cell **21:** 3152–3169.

Lomin, S.N., Krivosheev, D.M., Steklov, M.Y., Osolodkin, D.I., and Romanov, G.A. (2012). Receptor properties and features of cytokinin signaling. Acta Naturae **4:** 31–45.

Mähönen, A.P., Bishopp, A., Higuchi, M., Nieminen, K.M., Kinoshita, K., Törmäkangas, K., Ikeda, Y., Oka, A., Kakimoto, T., and Helariutta, Y. (2006). Cytokinin signaling and its inhibitor AHP6 regulate cell fate during vascular development. Science **311:** 94–98.

Marhavý, P., Duclercq, J., Weller, B., Feraru, E., Bielach, A., Offringa, R., Friml, J., Schwechheimer, C., Murphy, A., and Benková, E. (2014). Cytokinin controls polarity of PIN1-dependent auxin transport during lateral root organogenesis. Curr. Biol. **24:** 1031–1037.

Matsumoto-Kitano, M., Kusumoto, T., Tarkowski, P., Kinoshita-Tsujimura, K., Václavíková, K., Miyawaki, K., and Kakimoto, T. (2008). Cytokinins are central regulators of cambial activity. Proc. Natl. Acad. Sci. USA **105:** 20027–20031.

Miyawaki, K., Matsumoto-Kitano, M., and Kakimoto, T. (2004). Expression of cytokinin biosynthetic isopentenyltransferase genes in *Arabidopsis*: tissue specificity and regulation by auxin, cytokinin, and nitrate. Plant J. **37:** 128–138.

Miyawaki, K., Tarkowski, P., Matsumoto-Kitano, M., Kato, T., Sato, S., Tarkowska, D., Tabata, S., Sandberg, G., and Kakimoto, T. (2006). Roles of *Arabidopsis* ATP/ADP isopentenyltransferases and tRNA isopentenyltransferases in cytokinin biosynthesis. Proc. Natl. Acad. Sci. USA **103:** 16598–16603.

Moreira, S., Bishopp, A., Carvalho, H., and Campilho, A. (2013). AHP6 inhibits cytokinin signaling to regulate the orientation of pericycle cell division during lateral root initiation. PLoS One **8:** e56370.

Motyka, V., Faiss, M., Strand, M., Kamínek, M., and Schmülling, T. (1996). Changes in cytokinin content and cytokinin oxidase activity in response to derepression of *ipt* gene transcription in transgenic tobacco calli and plants. Plant Physiol. **112:** 1035–1043.

Müller, B., and Sheen, J. (2008). Cytokinin and auxin interaction in root stem-cell specification during early embryogenesis. Nature **453:** 1094–1097.

Nishimura, C., Ohashi, Y., Sato, S., Kato, T., Tabata, S., and Ueguchi, C. (2004). Histidine kinase homologs that act as cytokinin receptors possess overlapping functions in the regulation of shoot and root growth in Arabidopsis. Plant Cell **16:** 1365–1377.

Pěnčík, A., et al. (2013). Regulation of auxin homeostasis and gradients in *Arabidopsis* roots through the formation of the IAA catabolite oxIAA. Plant Cell **25:** 3858–3870.

Petersson, S.V., Johansson, A.I., Kowalczyk, M., Makoveychuk, A., Wang, J.Y., Moritz, T., Grebe, M., Benfey, P.N., Sandberg, G., and Ljung, K. (2009). An auxin gradient and maximum in the *Arabidopsis* root apex shown by high-resolution cell-specific analysis of IAA distribution and synthesis. Plant Cell **21:** 1659–1668.

Petricka, J.J., Schauer, M.A., Megraw, M., Breakfield, N.W., Thompson, J.W., Georgiev, S., Soderblom, E.J., Ohler, U., Moseley, M.A., Grossniklaus, U., and Benfey, P.N. (2012). The protein expression landscape of the *Arabidopsis* root. Proc. Natl. Acad. Sci. USA **109:** 6811–6818.

Rappsilber, J., Ishihama, Y., and Mann, M. (2003). Stop and go extraction tips for matrix-assisted laser desorption/ionization, nanoelectrospray, and LC/MS sample pretreatment in proteomics. Anal. Chem. **75:** 663–670.

Rappsilber, J., Mann, M., and Ishihama, Y. (2007). Protocol for micro-purification, enrichment, pre-fractionation and storage of peptides for proteomics using StageTips. Nat. Protoc. **2:** 1896–1906.

Romanov, G.A., Lomin, S.N., and Schmülling, T. (2006). Biochemical characteristics and ligand-binding properties of Arabidopsis cytokinin receptor AHK3 compared to CRE1/AHK4 as revealed by a direct binding assay. J. Exp. Bot. **57:** 4051–4058.

Růžička, K., Simásková, M., Duclercq, J., Petrásek, J., Zazímalová, E., Simon, S., Friml, J., Van Montagu, M.C., and Benková, E. (2009). Cytokinin regulates root meristem activity via modulation of the polar auxin transport. Proc. Natl. Acad. Sci. USA **106:** 4284–4289.

Sakakibara, H. (2006). Cytokinins: activity, biosynthesis, and translocation. Annu. Rev. Plant Biol. **57:** 431–449.

Schaller, G.E., Bishopp, A., and Kieber, J.J. (2015). The yin-yang of hormones: cytokinin and auxin interactions in plant development. Plant Cell **27:** 44–63.

Schmitz, R.Y., and Skoog, F. (1972). Cytokinins: synthesis and biological activity of geometric and position isomers of zeatin. Plant Physiol. **50:** 702–705.

Spanswick, R.M., and Miller, A.G. (1977). Measurement of the cytoplasmic pH in *Nitella translucens*: Comparison of values obtained by microelectrode and weak acid methods. Plant Physiol. **59:** 664–666.

Spíchal, L., Rakova, N.Y., Riefler, M., Mizuno, T., Romanov, G.A., Strnad, M., and Schmülling, T. (2004). Two cytokinin receptors of *Arabidopsis thaliana*, CRE1/AHK4 and AHK3, differ in their ligand specificity in a bacterial assay. Plant Cell Physiol. **45:** 1299–1305.

Spíchal, L. (2012). Cytokinins–recent news and views of evolutionarily old molecules. Funct. Plant Biol. **39:** 267–284.

Spiess, L.D. (1975). Comparative activity of isomers of zeatin and ribosyl-zeatin on *Funaria hygrometrica*. Plant Physiol. **55:** 583–585.

Svačinová, J., Novák, O., Plačková, L., Lenobel, R., Holík, J., Strnad, M., and Doležal, K. (2012). A new approach for cytokinin

isolation from *Arabidopsis* tissues using miniaturized purification: pipette tip solid-phase extraction. Plant Methods **8:** 17.

Swarup, R., Kramer, E.M., Perry, P., Knox, K., Leyser, H.M., Haseloff, J., Beemster, G.T., Bhalerao, R., and Bennett, M.J. (2005). Root gravitropism requires lateral root cap and epidermal cells for transport and response to a mobile auxin signal. Nat. Cell Biol. **7:** 1057–1065.

Takei, K., Ueda, N., Aoki, K., Kuromori, T., Hirayama, T., Shinozaki, K., Yamaya, T., and Sakakibara, H. (2004). AtIPT3 is a key determinant of nitrate-dependent cytokinin biosynthesis in *Arabidopsis.* Plant Cell Physiol. **45:** 1053–1062.

Tucker, E.B. (1993). Azide treatment enhances cell-to-cell diffusion in staminal hairs of *Setcreasea purpurea.* Protoplasma 174**:** 45–49.

Turnbull, C.G.N., and Hanke, D.E. (1985). The control of bud dormancy in potato tubers. Measurement of the seasonal pattern of changing concentrations of zeatin-cytokinins. Planta **165:** 366–376.

Wang, J., Ma, X.-M., Kojima, M., Sakakibara, H., and Hou, B.-K. (2013). Glucosyltransferase UGT76C1 finely modulates cytokinin responses via cytokinin N-glucosylation in *Arabidopsis thaliana.* Plant Physiol. Biochem. **65:** 9–16.

Werner, T., Motyka, V., Laucou, V., Smets, R., Van Onckelen, H., and Schmülling, T. (2003). Cytokinin-deficient transgenic *Arabidopsis* plants show multiple developmental alterations indicating opposite functions of cytokinins in the regulation of shoot and root meristem activity. Plant Cell **15:** 2532–2550.

Wulfetange, K., Lomin, S.N., Romanov, G.A., Stolz, A., Heyl, A., and Schmülling, T. (2011). The cytokinin receptors of *Arabidopsis* are located mainly to the endoplasmic reticulum. Plant Physiol. **156:** 1808–1818.

Yonekura-Sakakibara, K., Kojima, M., Yamaya, T., and Sakakibara, H. (2004). Molecular characterization of cytokinin-responsive histidine kinases in maize. Differential ligand preferences and response to *cis*-zeatin. Plant Physiol. **134:** 1654–1661.

Zatloukal, M., Gemrotová, M., Doležal, K., Havlícek, L., Spíchal, L., and Strnad, M. (2008). Novel potent inhibitors of *A. thaliana* cytokinin oxidase/dehydrogenase. Bioorg. Med. Chem. **16:** 9268–9275.

Zhang, K., Novák, O., Wei, Z., Gou, M., Zhang, X., Yu, Y., Yang, H., Cai, Y., Strnad, M., and Liu, C.J. (2014). *Arabidopsis* ABCG14 protein controls the acropetal translocation of root-synthesized cytokinins. Nat. Commun. **5:** 3274.

Zhang, W., Swarup, R., Bennett, M., Schaller, G.E., and Kieber, J.J. (2013). Cytokinin induces cell division in the quiescent center of the *Arabidopsis* root apical meristem. Curr. Biol. **23:** 1979–1989.

Zhang, W., To, J.P.C., Cheng, C.Y., Schaller, G.E., and Kieber, J.J. (2011). Type-A response regulators are required for proper root apical meristem function through post-transcriptional regulation of PIN auxin efflux carriers. Plant J. **68:** 1–10.

Zürcher, E., Tavor-Deslex, D., Lituiev, D., Enkerli, K., Tarr, P.T., and Müller, B. (2013). A robust and sensitive synthetic sensor to monitor the transcriptional output of the cytokinin signaling network *in planta.* Plant Physiol. **161:** 1066–1075.